2022 IEEE/RSJ International Conference on Intelligent Robots and Systems (IROS)
October 23-27, 2022, Kyoto, Japan

EMG-based Feedback Modulation for Increased Transparency in Teleoperation

Luc Schoot Uiterkamp[1], Francesco Porcini[2], Gwenn Englebienne[1], Antonio Frisoli[2], Douwe Dresscher[4]

***Abstract*— In interacting with stiff environments through teleoperated systems, time delays cause a mismatch between haptic feedback and the expected feedback by the operator. This mismatch causes artefacts in the feedback, which decrease transparency, but so does filtering these artefacts. Through modelling of operator stiffness and the expected feedback force with EMG, the artifacts can be selectively filtered without loss of transparency. We developed several feedback modulation techniques to bring the feedback force closer to the expected force: 1) the average between the modelled operator force and the feedback force, 2) a low pass filter and 3) a scaling modulation. To control for overdamping, a transparency check is included. We show that the averaging approach yields significantly better contacts than unmodulated feedback. None of the modulation algorithms differ significantly from the unmodulated feedback in transparency.**

I. Introduction

Teleoperation provides an intuitive tool that allows interaction with a remote environment. A teleoperation architecture is generally composed of a leader (a haptic device driven by the user) and an follower (a robotic device that interacts with the remote environment) connected through a communication channel, which allows the information exchange [1]. An effective teleoperation setup requires precise leader position tracking by the follower and a clear force feedback signal to ensure adequate dexterity and intuitiveness. However, the transparency requirements clash with the stability. For the sake of safety, stability must be ensured at the cost of transparency and many algorithms were developed to ensure this [2]–[5]. Performance of the control architecture can be improved by implementing solutions like position drift error compensation [6] or force-reference transparency enhancing solutions [7]. In a real implementation of a teleoperation architecture (*e.g.* for a disaster scenario response, like the one proposed in [8]), problems may arise when interacting with a stiff environment.

In particular, in *Position-Force (PF)* architectures interacting with stiff environments, the force feedback signal is delayed, which results in two possible scenarios. 1) As the operator pushes a follower against a stiff environment through manipulation of a leader, the follower makes contact with the environment before the leader can display a force to the operator. The lack of feedback causes the operator to continue applying force in order to further move the follower to make contact. This increases the force with which the follower pushes on the environment and in turn increases the feedback force, which causes an unexpectedly large force on the operator. As the contact has been established for longer than the operator was aware of, the feedback force will be displayed for longer than expected and with an unexpected amplitude. 2) If the operator stopped their effort and awaited the feedback without continued pushing of the leader, the stiffness of the operator's arm will decrease, as it is motionless in free space. This decreased arm stiffness causes a mismatch between the arm stiffness and the feedback force. This phenomenon decreases task performance while the operator attempts a transition from free space to a constrained contact with a stiff environment (*hard contact*), which is an often required task in teleoperation scenarios. Both these situations are due to the delay in the feedback channel and/or due to a mismatch in that delay.

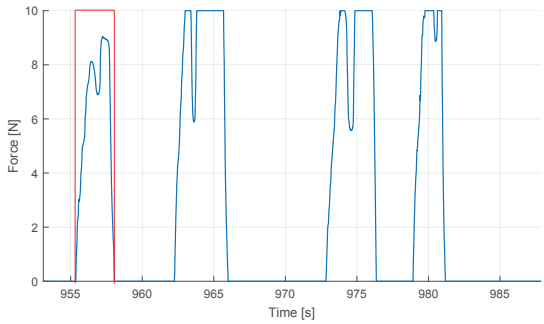

Fig. 1. The 'bounce' effect visible as dips in force as contact is made, with an ideal contact outlined in red.

The mismatch between the feedback force and the operator impedance causes the operator to be pushed back along with the leader, in some cases past the point in space where the contact was first established. This in turn causes the follower to move away from the environment. This failed transition between free space and a stable contact is referred to as a 'bounce' in this paper. This effect is clearly visible in figure 5 in Heck et al. [9], where an undamped contact transition leads to multiple bounces and is also visualised in figure 1 in this paper. The bounce effect is distinct from instabilities, which *can* cause similar effects, but differs from it because the mismatch between the human operator stiffness and the feedback force causes the bounce, not a force gain due to the architecture. The bounce problem has been reported in by many works in litterature [10], [11]. However, to the best knowledge of the authors, no specific solutions were

[1]Human Media Interaction, Faculty of Electrical Engineering, Mathematics and Computer Science, University of Twente, 7500 AE Enschede, The Netherlands l.schootuiterkamp@utwente.nl

[2]PERCRO Lab, Institute of Mechanical Intelligence, Scuola Superiore Sant'Anna, 56017, Ghezzano (San Giuliano Terme), Italy f.porcini@santannapisa.it

[4]Robotics and Mechatronics, Faculty of Electrical Engineering, Mathematics and Computer Science, University of Twente, 7500 AE Enschede, The Netherlands

2022 IEEE/RSJ International Conference on Intelligent Robots and Systems (IROS) | 978-1-6654-7927-1/22/$31.00 ©2022 IEEE | DOI: 10.1109/IROS47612.2022.9981162

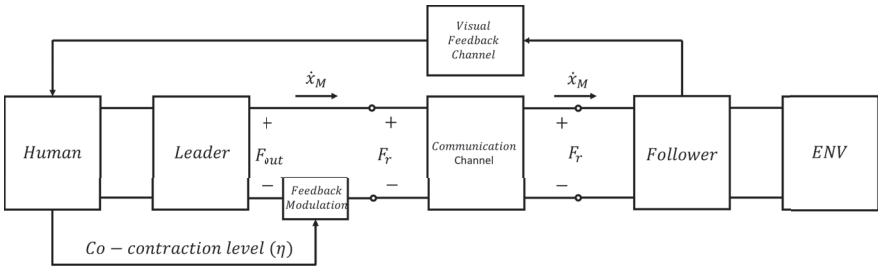

Fig. 2. Communication channels of the position force leader as used in this study, with feedback modulation.

proposed to address this problem.

These bounce effects can be greatly reduced by smoothing the force feedback displayed to the operator (*e.g.* [11] proposed over-damping the system to eliminate these bounces, without taking into account the operator state), giving the operator time to reestablish the correct stiffness to counteract the applied force at a cost in transparency (stiff environment may appear more compliant). Therefore, we propose three dynamic smoothing algorithms that only dampen the contact when there would otherwise be a bounce, improving stiff environment contact tasks effectiveness by facilitating a stable contact at a minimal loss of transparency. The impact on stability of this selective damping is not addressed and we assume an already stable *PF* architecture. To establish the effectiveness of these algorithms in decreasing the bounces, the contact shape is compared to an ideal contact shape in which no bounces are present, as visible by the red plot in figure 1, under each modulation condition. To assess the transparency of the modulation algorithms and to control for an overly large amount of damping, which decreases transparency, the ability of the operator to distinguish between a stiff and compliant environment is measured.

The paper is organized as follows: relevant related work is discussed in section II, the feedback modulation algorithms are outlined in section III and the study design section IV. The results are presented in section V and discussed in section VI.

II. Related work

Previous works aiming to improve transparency include adaptive impedance [12] and adaptive admittance [13] schemes, which improved tracking errors and intuitiveness by dynamically altering stiffness parameters which make the operation less cumbersome in free space and more precise in contact. In tele-impedance control, the impedance of the human arm is matched to the follower by estimating the arm impedance of the operator with EMG sensors and mimicking this on the follower [14]. The stiffness of the operator can be estimated by observing joint torques [15] or muscle activation [14]. Muscle activation measures have been used successfully for operator impedance estimation. Traditional wired electrode setups were used by [14], [16], [17] to measure muscle activity, but [18], [19] used wearable EMG sensors successfully. [14] use a simple linear mapping to relate muscle activation to stiffness, [18]–[20] use co-contraction as a direct stiffness indication, [16] uses a force model based on Stiffness Trend Index (STI, from [15]) to estimate force based on EMG values and velocity. All these approaches have in common that they assume the arm impedance does not change over the course of the time delay, and that as such the feedback force matches the arm impedance as it is displayed to the operator. As the impedance of the operator and follower are the same, the operator will receive a feedback force which fits the stiffness of the arm and no bounce effect will occur. However, in the presence of large time delays, the operator arm impedance can change, which causes a mismatch and consequently may cause a bounce. This work builds on the impedance estimation methods used in [15], [18]–[20] to estimate the impedance of the operator *after* the delayed feedback has arrived at the operator to match the feedback to the operator impedance.

III. Feedback modulation

In a *PF* teleoperation architecture the leader commands a position to the follower and the follower sends a reference force from a sensor back. When providing the user with the force directly from the sensor (referred to as *raw force* from now on), the user's stiffness is not taken into account. The arm stiffness provides an indirect measure of the force expected by the user and usually depends on the visual feedback and on past experiences. This expected force can be used as additional information to enhance the feedback to the user. In this section, we present three algorithms which modulate raw force using EMG-based estimated arm stiffness to take into account what the user expects. The objective is to provide the user with the best feedback information to accomplish a certain task. The modulation algorithms are developed to accomplish a 1-DoF task, but can be expanded to cover more degrees of freedom at the cost of greater complexity in terms of estimated stiffness. A schematic representation of the architecture is shown in figure 2. It should be noted that the force feedback communication channel does not exhibit time delay, thus the architecture is assumed to be stable (neglecting quantization and discretization effects) and only the quality of the feedback needed to accomplish a certain task is investigated in this paper. However, in order for bounces to occur, visual feedback and force feedback must be made asynchronous. In this way, no delay in the communication channel (but on visual feedback channel, see figure 2) guarantees a stable architecture and subject to bounces that cannot be confused with instability.

The feedback modulation algorithms are named *Average*, *Scale* and *Low-Pass Filter*. The first two algorithms require

a stiffness model (described below).

A. Stiffness model

The stiffness estimate is based on flexor (f) and extensor (e) EMG values which were low-pass (Butterworth) filtered to 2 Hz, biased to be relative to the initial value and normalized [18], [20]. The shared component of the activation $\epsilon_i(t)$ of antagonistic muscles is defined as the co-contraction $\eta(t)$. ϵ_{min_i} and ϵ_{max_i} are the minimum and maximum muscle activation levels collected during the EMG calibration. Time dependence is omitted for the sake of readability.

$$\begin{aligned} \hat{\epsilon}_i &= max\left(0, \frac{\epsilon_i - \epsilon_{min_i}}{\epsilon_{max_i} - \epsilon_{min_i}}\right) \text{ with } i = f, e \\ \eta &= min\left(\hat{\epsilon}_f, \hat{\epsilon}_e\right) \end{aligned} \tag{1}$$

Minimum and maximum muscle activations are recorded during a user-dependent calibration phase (see section IV-A), along with minimum (η_{min}) and maximum (η_{max}) co-contraction levels.

B. Feedback Modulation Strategies

The following strategies modulate the raw force (F_r) on the base of the co-contraction η. The output is a modulated force F_{out} which is commanded to the leader and then displayed to the user. All strategies have sampling rate $dt = \frac{1}{1000}[s]$. A maximum displayable force $F_{MAX} = 10\ [N]$ is assumed due to hardware limitations (see section IV).

1) Average: The *average* strategy computes an average between the raw force and the expected force. The force model presented in [16] was used to estimate the expected force the participant can be subjected to with acceptable deflection from the co-contraction value:

$$\begin{aligned} \hat{k}_h(t) &= \alpha \cdot \eta(t) + \beta\ [N/m] \rightarrow \text{estimated stiffness} \\ \hat{b}_h(t) &= \gamma \cdot \eta(t) + \delta\ [Ns/m] \rightarrow \text{estimated damping} \\ \Rightarrow F_m(t) &= \hat{k}_h(t) \cdot Dx(t) - \hat{b}_h(t) \cdot \dot{x}(t)\ [N] \end{aligned} \tag{2}$$

where $Dx(t) = (x(t) - x(t-1))$ denotes a position difference, $\dot{x}(t)$ a velocity and α, β, γ and δ are user-specific factors to be identified (see section IV-A). Position difference, velocity and force are recorded along with the EMG co-contraction signal for a certain amount of time T. Then, a linear regression problem is solved:

$$\begin{bmatrix} F_0 \\ F_1 \\ \vdots \\ F_T \end{bmatrix} = \begin{bmatrix} \eta_0 \cdot Dx_0 & Dx_0 & -\eta_0 \cdot \dot{x}_0 & -\dot{x}_0 \\ \eta_1 \cdot Dx_1 & Dx_1 & -\eta_1 \cdot \dot{x}_1 & -\dot{x}_1 \\ \vdots & \vdots & \vdots & \vdots \\ \eta_T \cdot Dx_T & Dx_T & -\eta_T \cdot \dot{x}_T & -\dot{x}_T \end{bmatrix} \begin{bmatrix} \alpha \\ \beta \\ \gamma \\ \delta \end{bmatrix}$$

$$\Rightarrow \begin{bmatrix} \alpha \\ \beta \\ \gamma \\ \delta \end{bmatrix} = \begin{bmatrix} \eta_0 \cdot Dx_0 & Dx_0 & -\eta_0 \cdot \dot{x}_0 & -\dot{x}_0 \\ \eta_1 \cdot Dx_1 & Dx_1 & -\eta_1 \cdot \dot{x}_1 & -\dot{x}_1 \\ \vdots & \vdots & \vdots & \vdots \\ \eta_T \cdot Dx_T & Dx_T & -\eta_T \cdot \dot{x}_T & -\dot{x}_T \end{bmatrix}^{+} \begin{bmatrix} F_0 \\ F_1 \\ \vdots \\ F_T \end{bmatrix} \tag{3}$$

where subscripts indicate time instants. The average modulation condition averages between the estimated force the operator is able to withstand and the raw force using an empirically chosen weight function $w(t)$ that depends on the co-contraction level:

$$\begin{aligned} F_{out}(t) = B(t) \cdot (&w(t) \cdot F_r(t) + \\ &(1 - w(t) \cdot F_m(t)) + i(t) + 0.5 \cdot F_r(t)\ [N] \\ w(t) = &\frac{e^{2 \cdot \eta(t)} - 1}{e^2 - 1}\ [\,] \rightarrow \text{weight} \end{aligned} \tag{4}$$

where $i(t)$ is an integral correction and $B(t)$ is a scaling correction:

$$\begin{aligned} E(t) &= F_r(t) - F_{out}(t)\ [N] \\ i(t) &= dt \cdot k \cdot E(t-1) + i(t-1)\ [N] \rightarrow \text{integrator} \\ B(t) &= \frac{F_{MAX} - 0.5 \cdot F_r(t) - i(t)}{F_{MAX}}\ [\,] \rightarrow \text{scaling factor} \end{aligned} \tag{5}$$

with $k = 5\ [1/s]$, which is an empirically set gain. The integral term is a correction which was added to ensure that the steady state value measured by the sensor is reached. If during a contact the user does not keep contracting their muscles, the modulated algorithm could provide them with a force which is lower than the sensor force. Thus, after a first modulated strike, the force should keep increasing up to the sensed value and this is realized with the integral correction. The term $B(t)$ is a scale to normalize the output force according to the maximum displayable force.

2) Scale: The scale strategy scales the raw force with the co-contraction level, yielding the presented output force:

$$\begin{aligned} F_{out}(t) &= B(t) \cdot w(t) \cdot F_r(t) + i(t) + 0.5 \cdot F_r(t)\ [N] \\ w(t) &= \frac{e^{2 \cdot \eta(t)} - 1}{e^2 - 1}\ [\,] \rightarrow \text{weight} \end{aligned} \tag{6}$$

Correction terms are the same used in equation 5.

3) Low-Pass Filter (LPF): The LPF modulation modifies the frequency contribution of the raw force based on the co-contraction. As the relation between the muscle co-contraction level and force is approximately linear [21], the co-contraction level $\eta(t)$ linearly maps the filter cutoff frequency between $\omega_{min} = 1Hz$ and $\omega_{max} = 20Hz$. This bandwidth was chosen in as it relates to the bandwidth of the kinesthetic perception capabilities of human body [22].

$$\begin{aligned} F_{out}(t) = F_{out}(t-1) &+ (F_r(t) - F_{out}(t-1)) \cdot \\ &(1 - e^{-dt \cdot 2\pi \cdot \omega(t)})\ [N] \\ &\begin{cases} m = \frac{\omega_{max} - \omega_{min}}{\eta_{max} - \eta_{min}}\ [rad/(V \cdot s)] \rightarrow \text{slope} \\ q = \omega_{max} - m \cdot \eta_{max}\ [rad/s] \rightarrow \text{offset} \\ \omega(t) = m \cdot \eta(t) + q\ [rad/s] \rightarrow \text{cutoff frequency} \end{cases} \end{aligned} \tag{7}$$

In this formulation, no integral correction is needed since the raw force is only modified in terms of frequency and not in amplitude.

IV. Method

A. EMG calibration

To obtain individualized parameters for the force model used in the averaging modulation algorithm, a short calibration was performed. Using the Omega 7 leader with constraints in place to limit the movement to 1 DoF, subjects pushed against a virtual wall with stiffness 500Nm with the pushing motion which was shown in a video beforehand. Over the course of 60 seconds, the cocontraction values, displayed force and position relative to the virtual wall were recorded at 1 kHz. The α, β, δ and ϵ values were calculated as described in section III-A.

B. Contact quality

For the contact quality assessment part of the study, subjects contacted a rigid surface six times per time delay condition and per feedback modulation condition resulting in a total of 72 contacts. Time delays were 0ms, 150ms and 300ms of visual delay on the monitor, while the haptic feedback remained undelayed to prevent instability from affecting the contacts. To distribute possible learning effects remaining after the familiarisation over the different conditions, the contacts were made in two rounds of three contacts each. In addition to this, the order of the feedback modulation conditions were randomly assigned per participant. The contact quality measure Δ is defined by

$$\Delta^i = \sum_{t_s^i}^{t_e^i} |F_{avg}^i - F_t^i| \, dt \tag{8}$$

where t_s^i and t_e^i are the start and end time for each contact i and F_{avg}^i is the average contact force during the contact. This measure was used, as the force in an ideal contact has very little deviation from the mean and the deviation increases as the number of bounces or the bounce size increases.

A bayesian linear model with the delay conditions, feedback modulation conditions and the participants as random effects and the feedback force grouped per time delay as conditional effect was used to determine the effect size of the conditions while controlling for individual differences and the lower force applied at higher time delays. A non-informative prior was used for this model, and as the deviation from the mean has a minimum of zero and no (theoretical) maximum, an exponential model family was chosen.

C. Transparency check

To determine the impact of the feedback modulation on the transparency of the system, participants were presented with a stiff and a compliant target in random order and were asked to differentiate between the two. The duration and number of contacts necessary for participants to distinguish between the targets were used as measures of transparency. The differentiation task was performed with the same delay and feedback modulation conditions as the contact quality part of the study. To ensure that the difference between targets could not be seen on the monitor despite the measures taken, 10 participants performed the differentiation task without any visual feedback in addition to the three time delay conditions. The effect of the time delay conditions on the number of contacts and on the time the subjects took to perform the task were compared with bayesian models. The delay conditions, the feedback modulation conditions and the participants were considered random effects in both the *number of contacts* and in the *time on task* models. In both models, a non-informative prior was used. For the *number of contacts* model, the poisson distribution family was chosen, as the outcome variable was discrete with a lower boundary. For the *time on task* model, an exponentially modified gaussian model family was chosen as the outcome variable is continuous with a non-zero lower bound.

Fig. 3. Setup of the user experiments. Left: user operating Omega 7 leader and wearing Myo EMG sensor. Right: user view of the robot end effector (left side of image), with alignment square, facing the contact target (right side of image).

D. Setup

An impedance controlled Franka Emika Panda arm was used to perform the movements, with a constant linear stiffness of 1000 Nm on the end effector. During the study, the arm was limited to two degrees of freedom: the main movement axis and the vertical axis to allow on-the-fly drift compensation by the operator. A Force Dimension Omega 7 was used as leader. The leader was mechanically constrained such that it was limited to one degree of freedom during experiments but could be lifted out of the alignment structure to realign the robot. An ATI mini-40 force torque sensor was used to provide force sensing for the force feedback. The setup was operated through ROS Kinetic at 1 kHz.

Figure 3 shows the Omega 7 in use on the left image and the end effector on the right image. The leader was operated with the subjects seated and resting their elbow on the chair armrest. The subjects were instructed to move the leader forward and backward with their wrist rather than with the full arm, as this facilitated EMG measurement at the arm. A Thalmic labs Myo armband (as used in [18]) was used to obtain raw EMG values from the wrist extensor and flexor muscles. The device can be seen on the arm of the subject in the left image in figure 3.

Subjects were instructed to hit a round target of 60mm in diameter (figure 3, right side on right image) with the end effector (figure 3, left side on right image). Two targets were made, one with a high stiffness and one with a low stiffness. The high stiffness target was used during the testing of the contact quality, both targets were used in the transparency check.

The targets were 3D-printed disks, the low stiffness target was made of a flexible plastic (TPU) with a very low infill to make it compliant, the high stiffness target was made of a

stiff plastic (PLA) with one layer of TPU on the outside to make the targets look identical. Subjects viewed the robot on a monitor through a livestream, which enabled a time delay to be set on the visual channel. The robot was shown from the side with a slight angle to the back so that the front of the targets could not be seen to prevent a visual identification of the stiffness of the target. An alignment square was placed on the monitor so that the end effector could be aligned such that the target would be struck in the center. Only adult competent subjects were recruited for this study. Subjects with any condition that lead them to be sensitive to injury on their dominant arm were excluded. A total of 19 subjects participated in the study of which 8 were female and 11 were male. All were right-handed.

Before the start of each user study, the following procedure was followed:

1) The researcher gave a short explanation of the goal of the study and the operation of the leader and the robot
2) The subject read the information brochure which details the same information and was given a chance to ask questions, after which subject signed the consent form
3) The subject watched a video which showed how the leader is best gripped, and what the length of the movements ought to be
4) The subject put on and aligned the EMG armband
5) The EMG armband calibration was performed
6) The subject practised moving the robot in different conditions for around five minutes to limit a later learning effect

V. Results

A. Contact quality

Two participants experienced significantly worse contacts than most participants, but these participants did not require more contacts or nor more time in the transparency check than other participants.

The posterior distributions and 90% credibility limits of the bayesian model for the effect of feedback modulation on the Δ measure (figure 4 and figure 5, right plot) show that, for all modulated conditions, Δ was lower than the raw condition. The *average* modulation yields the lowest Δ, with a mean of 2.07 (versus 2.49 for the raw condition) and $p(\Delta_{average} \geqslant \Delta_{raw}) = 0.036$. None of the delay conditions lead to a significantly higher or lower Δ than the raw condition (left plot in figure 5).

B. Transparency

The number of contacts required in the transparency task to determine the correct environment stiffness increased roughly linearly between 150ms and 300ms delay conditions and the condition with no visual feedback (figure 6, top left). The time spent on the task (ToT) was somewhat higher for the 300ms delay condition ($p(tot_{300ms} \geqslant tot_{0ms}) = 0.6$) but not for the 150 ms delay condition and the condition with no visual feedback (figure 6, top right). The number of contacts required to perform the transparency task in the *low pass* and *scale* conditions was roughly equal to the number

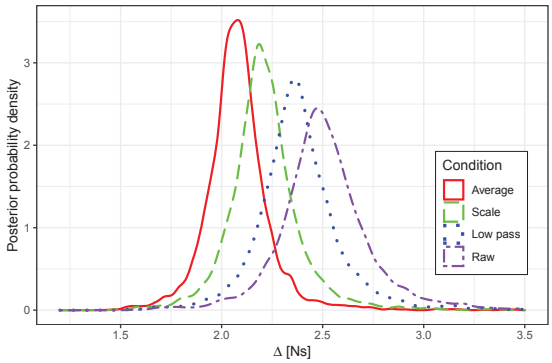

Fig. 4. Posterior probability distributions of effect of different modulation conditions on Δ.

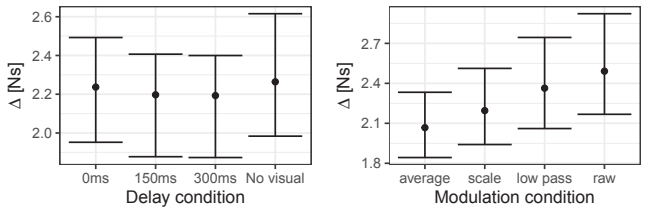

Fig. 5. Mean effects and 90% credibility limits for the delay conditions (left) and feedback modulation conditions (right) on Δ

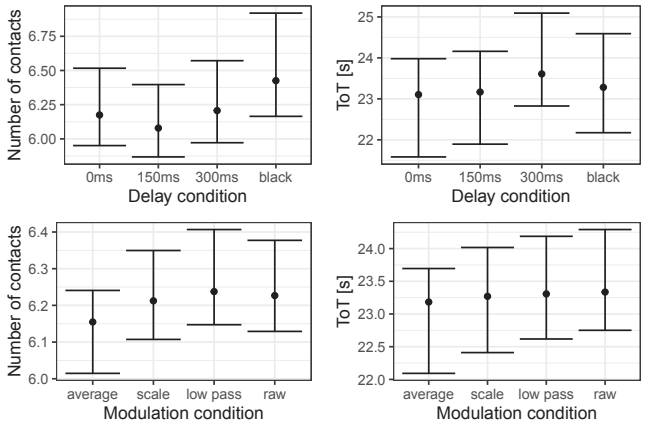

Fig. 6. Mean effects and 90% credibility limits for delay conditions (upper plots) and feedback modulation conditions (lower plots) on number of contacts (left plots) and time on task (ToT, right plots)

of contacts in the raw condition. The *average* modulation required somewhat fewer contacts (figure 6, bottom left), with $p(N_{average} \geqslant N_{raw}) = 0.17$. The ToT in the *low pass* and *scale* conditions was roughly equal to that of the raw condition, the ToT in the *average* condition was not significantly lower than in the raw condition (figure 6, bottom right) with $p(tot_{average} \geqslant tot_{raw}) = 0.82$.

VI. Discussion And Conclusions

There were two subjects who experienced significantly worse contacts than the others. The reason(s) for this are unclear. While these subjects had a reasonable knowledge about robotics, other participants who did not experience such bad contacts had this as well. As the study concerned physiological responses, knowledge about robotics was not considered an exclusion criterion. In addition to this, the

outlier subjects had no specific knowledge about the modulation algorithms being tested. The subjects were therefore not considered anomalies and were retained in the data for the analyses. The number of contacts in the condition with no visual feedback were slightly higher than the other delay conditions, but increased with the same trend as the 300ms condition with regards to the 150ms condition. The time on task for the condition with no visual feedback did not increase with the same trend, and lied between the 150ms and 300ms delay conditions. The lack of significant increase in either measure indicates that subjects were not able to visually deduce the stiffness of the target and that therefore all data could be used. As such the condition with no visual feedback is considered a large delay. The absence of significant effect of delay conditions on the Δ measure and number of contacts indicates that scenario #2 as described in section I is the main way of dealing with discrepant delay, as the time spent in free space does not influence the arm stiffness. The main goal of this study was to evaluate three feedback modulation algorithms and compare performance in a state transition from free space to a constrained contact. All modulation conditions brought the contact shape closer to the ideal (square) contact, but the *averaging* algorithm showed the most significant improvement, with a 17% drop in the mean effect size and a high certainty of improved performance. As the *scale* algorithm is very similar to the *average* algorithm except for the use of the user impedance model (eq. 2), the impedance model seems to add significant value. To evaluate whether the algorithms did not overdampen the feedback, possibly increasing contact quality but at a loss of transparency, a transparency check was performed. The time on task and number of contacts required to perform the transparency test are lower for the *averaging* condition than for the unmodulated condition. This indicates that the *averaging* algorithm indeed increased the transparency, and made it easier for subjects to identify the stiffness associated with the target. The *LPF* and *scale* algorithms performed on par with the unmodulated condition for both the time on task and number of contact measures. This means that, even though the contact quality improved somewhat, the transparency did not increase, which is an indication of overdamping. In this study, the base controller had a fixed impedance. In combination with the high time delays on the visual modality, impedance mismatch was very likely to occur. As the feedback modulation is a last-second repair of a mismatched impedance, it is best combined with an adaptive tele-impedance setup to match the impedance of the operator and actuator. This ensures that there is only as much damping as is necessary to ensure good quality contacts and minimized overdamping.

REFERENCES

[1] D. A. Lawrence, "Stability and transparency in bilateral teleoperation," in *[1992] Proceedings of the 31st IEEE Conference on Decision and Control*. IEEE, 1992, pp. 2649–2655.

[2] R. J. Anderson and M. W. Spong, "Bilateral control of teleoperators with time delay," in *Proceedings of the 1988 IEEE International Conference on Systems, Man, and Cybernetics*, vol. 1. IEEE, 1988, pp. 131–138.

[3] G. Niemeyer and J.-J. Slotine, "Stable adaptive teleoperation," *IEEE Journal of oceanic engineering*, vol. 16, no. 1, pp. 152–162, 1991.

[4] P. F. Hokayem and M. W. Spong, "Bilateral teleoperation: An historical survey," *Automatica*, vol. 42, no. 12, pp. 2035–2057, 2006.

[5] J.-H. Ryu, Y. S. Kim, and B. Hannaford, "Sampled-and continuous-time passivity and stability of virtual environments," *IEEE Transactions on Robotics*, vol. 20, no. 4, pp. 772–776, 2004.

[6] A. Coelho, H. Singh, T. Muskardin, R. Balachandran, and K. Kondak, "Smoother position-drift compensation for time domain passivity approach based teleoperation," in *2018 IEEE/RSJ International Conference on Intelligent Robots and Systems (IROS)*. IEEE, 2018, pp. 5525–5532.

[7] H. Singh, A. Jafari, and J.-H. Ryu, "Enhancing the force transparency of time domain passivity approach: Observer-based gradient controller," in *2019 International Conference on Robotics and Automation (ICRA)*. IEEE, 2019, pp. 1583–1589.

[8] T. Klamt, D. Rodriguez, L. Baccelliere, X. Chen, D. Chiaradia, T. Cichon, M. Gabardi, P. Guria, K. Holmquist, M. Kamedula *et al.*, "Flexible disaster response of tomorrow: Final presentation and evaluation of the centauro system," *IEEE robotics & automation magazine*, vol. 26, no. 4, pp. 59–72, 2019.

[9] D. Heck, A. Saccon, R. Beerens, and H. Nijmeijer, "Direct Force-Reflecting Two-Layer Approach for Passive Bilateral Teleoperation with Time Delays," *IEEE Transactions on Robotics*, vol. 34, no. 1, pp. 194–206, 2018.

[10] J.-H. Ryu, D.-S. Kwon, and B. Hannaford, "Stable teleoperation with time-domain passivity control," *IEEE Transactions on robotics and automation*, vol. 20, no. 2, pp. 365–373, 2004.

[11] S. Sirouspour and A. Shahdi, "Model predictive control for transparent teleoperation under communication time delay," *IEEE Transactions on Robotics*, vol. 22, no. 6, pp. 1131–1145, 2006.

[12] R. Colbaugh, H. Seraji, and K. Glass, "Direct adaptive impedance control of manipulators," *Proceedings of the IEEE Conference on Decision and Control*, vol. 3, pp. 2410–2415, 1991.

[13] H. Seraji, "Adaptive admittance control: an approach to explicit force control in compliant motion," *Proceedings - IEEE International Conference on Robotics and Automation*, no. pt 4, pp. 2705–2710, 1994.

[14] A. Ajoudani, N. Tsagarakis, and A. Bicchi, "Tele-impedance: Teleoperation with impedance regulation using a body-machine interface," *International Journal of Robotics Research*, vol. 31, no. 13, pp. 1642–1655, 2012.

[15] N. Karavas, A. Ajoudani, N. Tsagarakis, J. Saglia, A. Bicchi, and D. Caldwell, "Tele-impedance based assistive control for a compliant knee exoskeleton," *Robotics and Autonomous Systems*, vol. 73, pp. 78–90, 2015.

[16] M. Laghi, A. Ajoudani, M. Catalano, and A. Bicchi, "Tele-impedance with force feedback under communication time delay," *IEEE International Conference on Intelligent Robots and Systems*, vol. 2017-September, pp. 2564–2571, 2017.

[17] Z. Li, Z. Huang, W. He, and C. Y. Su, "Adaptive impedance control for an upper limb robotic exoskeleton using biological signals," *IEEE Transactions on Industrial Electronics*, vol. 64, no. 2, pp. 1664–1674, 2017.

[18] K. Van Teeffelen, D. Dresscher, W. Van Dijk, and S. Stramigioli, "Intuitive Impedance Modulation in Haptic Control Using Electromyography," *Proceedings of the IEEE RAS and EMBS International Conference on Biomedical Robotics and Biomechatronics*, vol. 2018-Augus, pp. 1211–1217, oct 2018.

[19] J. Chen, M. Glover, C. Li, and C. Yang, "Development of a user experience enhanced teleoperation approach," *ICARM 2016 - 2016 International Conference on Advanced Robotics and Mechatronics*, pp. 171–177, 2016.

[20] D. S. Walker, R. P. Wilson, and G. Niemeyer, "User-controlled variable impedance teleoperation," *Proceedings - IEEE International Conference on Robotics and Automation*, pp. 5352–5357, 2010.

[21] R. Osu and H. Gomi, "Multijoint muscle regulation mechanisms examined by measured human arm stiffness and EMG signals," *Journal of Neurophysiology*, vol. 81, no. 4, pp. 1458–1468, 1999.

[22] A. E. Saddik, M. Orozco, M. Eid, and J. Cha, *Human Haptic Perception*. Berlin, Heidelberg: Springer Berlin Heidelberg, 2011, pp. 45–66.